Journal of Zhejiang University-SCIENCE A 2026 27(10):1181-1194
www.jzus.zju.edu.cn; www.springer.com/journal/11582
E-mail: jzus_a@zju.edu.cn

Research Article
https://doi.org/10.1631/jzus.A2600078

Check for updates

Subbranch circuit approach for controlling neuronal dynamics in a memristive Josephson system

Ying XU[1]✉, Fuqiang WU[2]

[1]*School of Mathematics and Statistics, Shandong Normal University, Jinan 250014, China*
[2]*School of Mathematics and Statistics, Ningxia University, Yinchuan 750021, China*

Abstract: The dynamic behavior of memristive Josephson neurons is highly sensitive to circuit configurations. This study proposes a novel control method for neuronal circuits based on targeted parallel shunting using an external capacitor. A hybrid circuit integrating a memristor, a Josephson junction, and a nonlinear resistor is constructed, with an external capacitive branch introduced in parallel with the nonlinear resistor to achieve precise manipulation of neuronal firing patterns. It is demonstrated that the external capacitive branch enables effective regulation of the firing patterns of the neuronal circuit through its targeted parallel connection to the nonlinear resistor. By continuously adjusting the external capacitance parameter, the system can realize controllable switching among various firing modes. Concurrently, variations in the stimulus amplitude reshape the internal energy distribution framework of the system, determining the dominant roles of different energy storage components. These two mechanisms constitute a dual-dimensional "mode–energy" regulation system for the neuronal circuit. Furthermore, the regulatory mechanism of the external branch originates from its unique local shunting effect and specific energy exchange process. The energy evolution of the external capacitor exhibits dynamic characteristics distinct from those of the main system, and this asynchronous energy response can effectively perturb the global balance of the system. The proposed method provides a foundation for the precise control of neuronal dynamics in memristive Josephson systems.

Key words: Neuronal dynamics; Capacitive subbranch; Firing mode regulation; Energy distribution

1 Introduction

With the rapid advancement of neuromorphic computing and brain-computer interface technologies, there is an escalating demand for the precise regulation of neuronal dynamics. The electrical activities of biological neurons stem from the stochastic diffusion of intracellular and extracellular ions and their bidirectional pumping across membrane channels. These processes are accompanied by energy exchange between magnetic and electric fields inside and outside the cell membrane, as well as variations in electromagnetic energy (Buzsáki and Draguhn, 2004; Uhlhaas and Singer, 2006; Ranasinghe et al., 2022). Neuronal populations form intricate networks through synaptic coupling. Their synchronous and asynchronous behaviors are not only integral to basic brain functions such as memory storage and signal integration but also closely linked to the pathological mechanisms of neurological disorders such as epilepsy and Parkinson's disease (Hodgkin and Huxley, 1952; Izhikevich, 2006; Zhao et al., 2024). Thus, constructing physical models capable of accurately replicating the dynamical characteristics of biological neurons and developing efficient regulation methods have become central research directions in neuromorphic computing and neuroengineering. Memristors, distinguished by their variable resistance, nonvolatility, and long- and short-term memory effects, can efficiently simulate synaptic weight modifications and neuronal electrical dynamical processes. This makes them key components for building low-power, high-density brain-inspired hardware systems (Chua, 1971; Strukov et al., 2008; Prezioso et al., 2015). Their unique nonlinear modulation and dynamic energy response capabilities enable precise reproduction of ion channel quantum transport and synaptic plasticity, thereby infusing neural circuits with more biologically realistic physical

✉ Ying XU, uryysunshine@163.com
Ying XU, https://orcid.org/0000-0002-8419-373X

Received Feb. 2, 2026; Revision accepted Apr. 22, 2026;
Crosschecked June 3, 2026; Online first July 21, 2026

© Zhejiang University Press 2026

mechanisms (Li et al., 2021; Xu et al., 2024; Lei and Ma, 2025). As core components of superconducting circuits, Josephson junctions exhibit quantum tunneling effects and electromagnetic coupling properties that can mimic the rapid switching behavior of ion channels, demonstrating unique advantages in reproducing high-frequency neuronal firing and enabling quantum regulation (Nakamura et al., 2001; Zhang et al., 2020; Baumgartner et al., 2022). Integrating memristors with Josephson junctions to form hybrid neural circuits can simultaneously balance dynamical richness and physical authenticity. This integration helps overcome the limitations of traditional models in describing quantum effects and energy coupling, thereby offering a novel technical pathway for regulating neuronal dynamics (Mishra et al., 2021; Wu et al., 2024; Yang et al., 2024).

Current regulation methods for neuronal circuits mainly rely on direct adjustments to main circuit parameters or external electrical signal injection, which suffer from inherent drawbacks such as limited precision, response lag, and substantial energy consumption (Guo et al., 2021; Han et al., 2023). Most existing studies focus on single-dimensional regulation of firing modes, overlooking the synergistic relationship between firing behavior and energy distribution (Lei et al., 2025a). Notably, mode switching in biological neurons is always accompanied by dynamic restructuring of metabolic energy, a core biophysical characteristic that traditional models often fail to effectively simulate (Wang and Zhang, 2007; Moujahid et al., 2011). Additionally, conventional circuit designs heavily depend on capacitors to mimic the capacitive properties of cell membranes (Sun et al., 2023). However, capacitors are prone to breakdown under strong electric shocks, leading to disrupted energy transmission and chaotic firing patterns, which restricts the stability of neural circuits under extreme operating conditions (Cheng et al., 2007; Moon and Leeb, 2016). Therefore, developing a regulation method that achieves precise switching of firing modes, controllable energy distribution, and interference resistance remains an urgent challenge in neuromorphic computing (Guo et al., 2025). The targeted integration of functional devices provides new insights for expanding the functionalities of neural circuits. In recent years, external subbranch circuits, through targeted coupling with the main circuit, have enabled dynamical regulation while preserving the main circuit topology. Their core advantage lies in flexibly adjusting the equivalent impedance and energy distribution of the main circuit via local shunting effects and energy exchange (Li et al., 2024). For instance, paralleling an external capacitive subbranch with a nonlinear resistor can modify transmembrane current characteristics through dynamic shunting, thereby inducing firing mode transitions (Jia et al., 2025). The introduction of functional devices such as piezoelectric materials and thermistors endows neural circuits with the ability to perceive multi-physical field stimuli, including sound, light, and temperature. This regulatory approach not only avoids direct modifications to the main circuit but also achieves reversible switching between multiple firing modes through continuous adjustment of a single parameter, offering a novel solution for circuit design under capacitor failure scenarios (Jia et al., 2023, 2024; Wang et al., 2024).

Notably, recent studies have shown that magnetic flux-controlled memristors (MFCMs), when integrated into neural circuit branches, can support energy shunting in the form of magnetic flux. This enables the description of magnetic field effects and the storage of magnetic flux variables in equivalent dimensionless neuron models (Lei et al., 2025b). MFCMs coupled with double capacitive membranes can detect external magnetic field fluctuations and alter the energy distribution (Jiang et al., 2025). Such MFCM-coupled circuits, combined with inductors, can realize continuous energy exchange relying solely on magnetic field components, overcoming the traditional requirement for oscillatory circuits to have energy interactions between electric and magnetic field storage elements (Liu et al., 2025). Meanwhile, Josephson junctions, in both resistive capacitive shunted and resistive capacitive inductively shunted models, exhibit neuron-like spiking and bursting behaviors (Dana et al., 2001). Their dynamical mechanisms can be interpreted through fold-homoclinic or parabolic bifurcations, further confirming their feasibility in simulating biological neuronal excitability (Laing, 2023). Recent studies have revealed new dynamical mechanisms, including spiking related to a saddle-node off invariant cycle bifurcation and a Josephson junction neuron model with phase-dependent memristive current (Baxevanis and Hizanidis, 2025; Yan et al., 2026). Moreover, dual-capacitor configurations have been shown to more accurately replicate the bilayer structure of biological cell membranes,

facilitating more realistic energy exchange between inner and outer membrane layers (Yang et al., 2024). A double-membrane neuron model with memcapacitors and memristors has been developed, showing that the capacitance ratio controls the degree of chaos (Lei et al., 2026). Furthermore, the synchronization dynamics of coupled Josephson junction-memristor systems are sensitive to coupling strength ratios, external stimulus parameters, and noise, underscoring the need for multidimensional regulatory strategies (Liu et al., 2025). Discrete neuron models and memristive neural network mapping have been reviewed recently (Yu et al., 2025). For Chinese researchers, please refer to the recent review (Ma, 2026) for further physical guidance on modeling and establishing neural circuits.

Thus, this study proposes a regulation method for neuronal dynamics in memristive Josephson systems based on targeted parallel shunting with an external capacitor. We systematically explore the regulatory laws of the external capacitance parameter on firing modes and clarify the core regulatory mechanisms of the local shunting effect and asynchronous energy response of the external branch. This study identifies two regulation dimensions. The mode dimension uses the parameter μ to switch among periodic, bursting, and chaotic firing. The energy dimension uses stimulus amplitude A to reshape the energy distribution and determine dominant components. Together, they form a dual-dimensional mode–energy regulation system for the neuron circuit. The research findings not only provide technical support for the precise regulation of neuronal dynamics in memristive Josephson systems but also lay a theoretical foundation for constructing reconfigurable, high-reliability neuromorphic circuits.

2 Modeling and methods

A controllable neuron circuit model is proposed, as illustrated in Fig. 1. The circuit consists of two distinct sections: the core neuron circuit and an external shunt-control branch (highlighted by the dashed box).

The core neuron circuit models the essential electrophysiological behaviors of a neuron. It is constructed around a Josephson junction J and a charge-controlled memristor M. A direct current voltage source E_1 and the memristor M are connected in series to form a

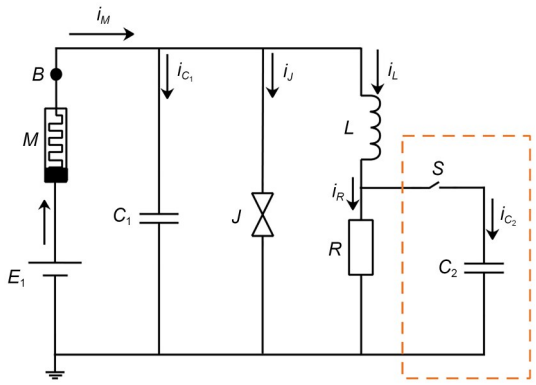


Fig. 1 Proposed controllable neuron circuit. The parameters are explained in the text

stimulation branch. Three parallel paths extend from their common node: the first incorporates a capacitor C_1, the second a Josephson junction J, and the third a nonlinear resistor R in series with an inductor L. The key innovation lies in the external shunt-control branch, which consists of an external capacitor C_2 and a switch S connected in series. This entire branch is connected in parallel with the nonlinear resistor in the core circuit. The switch S regulates the activation of this branch. The external capacitor C_2 is nonpolarized because the voltage across the nonlinear resistor R may reverse during dynamics. Therefore, no polarity symbol is indicated in Fig. 1.

2.1 Model derivation and nondimensionalization

The governing physical laws for each component are defined as follows. The memristor M is a magnetic flux-regulated device described by:

$$\begin{cases} i_M = W(\varphi)V_M, \\ \dfrac{\mathrm{d}\varphi}{\mathrm{d}t} = k_1 V_M + k_0 \varphi, \\ W(\varphi) = \alpha + 3\beta\varphi^2, \end{cases} \tag{1}$$

where $V_M = E_1 - V_B$ is the voltage across the memristor, E_1 is the voltage at node 1 (i.e., the direct current voltage source E_1), and V_B is the voltage at node B. i_M is the current through the memristor. φ is the magnetic flux. $W(\varphi)$ is the memductance. t is time. The parameters k_0, k_1, α, and β are constants. The Josephson junction obeys:

$$i_J = I_C \sin(\phi), \quad \frac{\mathrm{d}\phi}{\mathrm{d}t} = \frac{2e}{\hbar} V_B, \tag{2}$$

where I_C is the critical current, e is the elementary charge, $\hbar$ denotes the reduced Planck constant, i_J is the current through the Josephson junction, and ϕ is the phase difference across it.

The capacitor C_1 follows $i_{C_1}=C_1\mathrm{d}V_B/\mathrm{d}t$, where i_{C_1} is the current through C_1 and C_1 is its capacitance. The nonlinear resistor R is modeled using the FitzHugh–Nagumo (FHN) formalism:

$$i_R=-\frac{1}{\rho}\left(V_R-\frac{1}{3}\frac{V_R^3}{V_0^2}\right), \tag{3}$$

where ρ and V_0 are normalized parameters for the nonlinear resistor. i_R is the current through R and V_R is the voltage across it. The inductor L satisfies $V_L=L\mathrm{d}i_L/\mathrm{d}t$, where V_L is the voltage across the inductor, i_L is the current through it, and L is the inductance. The external capacitor C_2 contributes a current $i_{C_2}=C_2\mathrm{d}V_R/\mathrm{d}t$, where i_{C_2} is the current through C_2 and C_2 is its capacitance. The dynamical equations are derived by applying Kirchhoff's laws to the circuit in Fig. 1. Two distinct operational modes are considered, depending on the state of switch *S*.

2.1.1 Case 1: switch open

In this case, $i_{C_2}=0$ and $i_L=i_R$. Applying Kirchhoff's current law (KCL) at node B gives:

$$\begin{aligned} &i_M=i_J+i_{C_1}+i_L,\\ &\Rightarrow W(\varphi)(E_1-V_B)=I_C\sin(\phi)+C_1\frac{\mathrm{d}V_B}{\mathrm{d}t}+i_L. \end{aligned} \tag{4}$$

Applying Kirchhoff's voltage law (KVL) to the R–L loop gives:

$$V_B=V_R+L\frac{\mathrm{d}i_L}{\mathrm{d}t}, \tag{5}$$

where

$$\frac{\mathrm{d}i_R}{\mathrm{d}t}=\frac{\mathrm{d}i_R}{\mathrm{d}V_R}\frac{\mathrm{d}V_R}{\mathrm{d}t}=-\frac{1}{\rho}\left(1-\frac{V_R^2}{V_0^2}\right)\frac{\mathrm{d}V_R}{\mathrm{d}t}. \tag{6}$$

Substituting the component relations leads to the following set of ordinary differential equations:

$$\begin{cases} C_1\dfrac{\mathrm{d}V_B}{\mathrm{d}t}=(\alpha+3\beta\varphi^2)(E_1-V_B)-I_C\sin(\phi)-i_L,\\ \dfrac{\mathrm{d}i_L}{\mathrm{d}t}=\dfrac{1}{L}(V_B-V_R),\\ \dfrac{\mathrm{d}\phi}{\mathrm{d}t}=\dfrac{2e}{\hbar}V_B,\\ \dfrac{\mathrm{d}\varphi}{\mathrm{d}t}=k_1(E_1-V_B)+k_0\varphi,\\ i_L=-\dfrac{1}{\rho}\left(V_R-\dfrac{1}{3}\dfrac{V_R^3}{V_0^2}\right). \end{cases} \tag{7}$$

2.1.2 Case 2: switch closed

Now, the external capacitor C_2 is connected in parallel with R, so $V_{C_2}=V_R$ (V_{C_2} is the voltage across the capacitor C_2) and $i_{C_2}=C_2\mathrm{d}V_R/\mathrm{d}t$. The current through the inductor becomes $i_L=i_R+i_{C_2}$. KCL at node B is modified to:

$$\begin{aligned} &i_M=i_J+i_{C_1}+i_L,\\ &\Rightarrow W(\varphi)(E_1-V_B)=I_C\sin(\phi)+C_1\frac{\mathrm{d}V_B}{\mathrm{d}t}+i_L,\\ &\Rightarrow C_1\frac{\mathrm{d}V_B}{\mathrm{d}t}=W(\varphi)(E_1-V_B)-I_C\sin(\phi)-i_L. \end{aligned} \tag{8}$$

The equations can be written as a fifth-order system:

$$\begin{cases} C_1\dfrac{\mathrm{d}V_B}{\mathrm{d}t}=(\alpha+3\beta\varphi^2)(E_1-V_B)-I_C\sin(\phi)-i_L,\\ \dfrac{\mathrm{d}i_L}{\mathrm{d}t}=\dfrac{1}{L}(V_B-V_R),\\ \dfrac{\mathrm{d}\phi}{\mathrm{d}t}=\dfrac{2e}{\hbar}V_B,\\ \dfrac{\mathrm{d}\varphi}{\mathrm{d}t}=k_1(E_1-V_B)+k_0\varphi,\\ C_2\dfrac{\mathrm{d}V_R}{\mathrm{d}t}=i_L+\dfrac{1}{\rho}\left(V_R-\dfrac{1}{3}\dfrac{V_R^3}{V_0^2}\right). \end{cases} \tag{9}$$

To simplify the analysis, all variables and parameters are nondimensionalized using the following transformations:

$$\begin{aligned} &x=\frac{V_B}{V_0},\quad y=\frac{\rho i_L}{V_0},\quad z=\phi,\quad w=\frac{\varphi}{\rho C_1 V_0},\\ &v=\frac{V_R}{V_0},\quad a=\alpha\rho,\quad b=3\beta\rho(C_1\rho V_0)^2, \end{aligned}$$

$$\begin{aligned}&\gamma=\frac{\rho I_{\mathrm{C}}}{V_0},\quad c=\frac{2e\rho C_1V_0}{\hbar},\quad \eta=\frac{L}{\rho^2C_1},\\&\tau=\frac{t}{\rho C_1},\quad A=\frac{E_1}{V_0},\quad \kappa_m=k_1,\\&\kappa_0=k_0\rho C_1,\quad \mu=\frac{C_2}{C_1}.\end{aligned}\tag{10}$$

The resulting dimensionless systems with switch open are:

$$\begin{cases}\dfrac{\mathrm{d}x}{\mathrm{d}\tau}=(a+bw^2)(A-x)-\gamma\sin(z)-y,\\[2mm]\dfrac{\mathrm{d}y}{\mathrm{d}\tau}=\dfrac{1}{\eta}(x-v),\\[2mm]\dfrac{\mathrm{d}z}{\mathrm{d}\tau}=cx,\\[2mm]\dfrac{\mathrm{d}w}{\mathrm{d}\tau}=\kappa_m(A-x)+\kappa_0w,\\[2mm]y=-v+\dfrac{1}{3}v^3.\end{cases}\tag{11}$$

The resulting dimensionless systems with the switch closed are:

$$\begin{cases}\dfrac{\mathrm{d}x}{\mathrm{d}\tau}=(a+bw^2)(A-x)-\gamma\sin(z)-y,\\[2mm]\dfrac{\mathrm{d}y}{\mathrm{d}\tau}=\dfrac{1}{\eta}(x-v),\\[2mm]\dfrac{\mathrm{d}z}{\mathrm{d}\tau}=cx,\\[2mm]\dfrac{\mathrm{d}w}{\mathrm{d}\tau}=\kappa_m(A-x)+\kappa_0w,\\[2mm]\dfrac{\mathrm{d}v}{\mathrm{d}\tau}=\dfrac{1}{\mu}\left(y+v-\dfrac{1}{3}v^3\right).\end{cases}\tag{12}$$

In this model, the membrane potential is represented by $x(\tau)$.

In these equations, τ is the dimensionless time and A is the stimulus amplitude. x, y, z, w, and v represent the dimensionless state variables of the system. a, b, γ, c, η, κ_m, κ_0, and μ are dimensionless parameters corresponding to the normalized forms of the original circuit parameters.

2.2 Stability and bifurcation analysis

To understand the system's steady-state behavior and its stability, we first identify its equilibrium points. Setting all time derivatives to zero (for both switch states) yields a unified set of algebraic equations. The equilibrium point $\boldsymbol{E}^*=(x^*, w^*, z^*, y^*, v^*)$ is:

$$\begin{aligned}&x^*=0,\quad v^*=0,\quad y^*=0,\quad w^*=-\frac{\kappa_mA}{\kappa_0},\\&\sin z^*=\frac{(a+bw^{*2})A}{\gamma}=P.\end{aligned}\tag{13}$$

Due to the periodicity of $\sin z^*$, multiple equilibrium solutions exist in the z-direction, with the necessary existence condition $|P|\leqslant1$. Notably, closing switch S does not alter the equilibrium position because the external capacitor carries no current at steady state. The system is linearized around the equilibrium. For the switch-open case, the algebraic constraint $y=-(v-v^3/3)$ approximates $y\approx-v$ near $v^*=0$. Combined with $\eta\dot{y}=x-v$, we obtain $v\approx x$, reducing the system to a 3D ordinary differential equation (ODE) set. Its Jacobian matrix is:

$$\boldsymbol{J}_{\mathrm{off}}=\begin{pmatrix}-(a+bw^{*2})+1 & 2bw^*A & -\gamma\cos z^*\\ -\kappa_m & -\kappa_0 & 0\\ -c & 0 & 0\end{pmatrix}.\tag{14}$$

For the switch-closed case, the system is a 5D ODE set with the Jacobian matrix:

$$\boldsymbol{J}_{\mathrm{on}}=\begin{pmatrix}-(a+bw^{*2}) & 2bw^*A & -\gamma\cos z^* & -1 & 0\\ -\kappa_m & -\kappa_0 & 0 & 0 & 0\\ -c & 0 & 0 & 0 & 0\\ -1 & 0 & 0 & 0 & 1\\ 0 & 0 & 0 & \dfrac{1}{\mu} & -\dfrac{1}{\mu}\end{pmatrix}.\tag{15}$$

Let $B=\alpha+\beta w^{*2}$ and $D=\gamma\cos z^*$. For the switch-open case, the characteristic polynomial is $\lambda^3+p_1\lambda^2+p_2\lambda+p_3=0$ (λ is an eigenvalue), with the following coefficients:

$$\begin{cases}p_1=B+1+\kappa_0,\\p_2=(B+1)\kappa_0-D\kappa_m+2bw^*Ac,\\p_3=-\gamma\kappa_0c\cos z^*.\end{cases}\tag{16}$$

Applying the Routh–Hurwitz criterion, the necessary and sufficient conditions for asymptotic stability are as follows:

$$p_1>0,\quad p_3>0,\quad p_1p_2>p_3.\tag{17}$$

For the switch-closed case, the Jacobian $\boldsymbol{J}_{\mathrm{on}}$ contains an eigenvalue $\lambda=1/\mu>0$ due to the constraint

structure. This eigenvalue originates from the conversion of the algebraic constraint into a differential equation and corresponds to the normal direction of the constraint manifold. This indicates instability in the full 5D state space. However, this positive eigenvalue corresponds to an inherent constraint mode and does not affect the effective dynamics on the reduced slow manifold. The physical stability is still governed by the conditions derived for the switch-open case. The stability conditions have clear physical interpretations. Condition $p_1>0$ requires sufficient total damping, combining memristor conductance and flux decay. Condition $p_3>0$ demands that the flux decay direction opposes the sign of the Josephson junction phase cosine term, forming essential negative feedback. Condition $p_1p_2>p_3$ represents a comprehensive coupling constraint among parameters. System bifurcations occur under specific parameter variations. A saddle-node bifurcation occurs when $p_3=0$, typically corresponding to $\cos z^*=0$. A Hopf bifurcation occurs when $p_1p_2=p_3$ with $p_2>0$, where the equilibrium loses stability and gives rise to limited cycle oscillations corresponding to periodic neuronal spiking. The switch S introduces an external capacitor C_2, corresponding to the dimensionless parameter $\mu=C_2/C_1$. While not altering equilibrium positions or linear stability conditions, μ adds a slow degree of freedom that transforms the system from a 4D differential-algebraic equation (DAE) to a 5D ODE. This dimensional expansion enables fast-slow dynamics separation, potentially generating complex oscillatory patterns such as bursting after a Hopf bifurcation. Thus, switch S acts as a dynamic reconfiguration tool, enabling mode switching between simple and complex firing patterns and providing a foundation for reconfigurable computational functions in neuromorphic circuits. The analytical stability conditions derived here clarify the parameter dependence of the system's steady-state behavior and provide theoretical foundations for the spiking pattern transitions observed in subsequent numerical simulations. Under physically admissible initial conditions that exactly satisfy the algebraic constraint, that is, the initial value of x is determined by the voltage across R at the switching instant, this mode is not excited.

2.3 Energy formulation

The total field energy stored in the circuit is the sum of the energies in the capacitive, inductive, and memristive components. For the switch-off case,

$$W_{\text{on}}=\frac{1}{2}C_1V_B+\frac{1}{2}(\alpha\varphi+\beta\varphi^3)(E_1-V_B)+\frac{1}{2}Li_L^2, \quad (18)$$

and for the switch-on case,

$$\begin{aligned}W_{\text{off}}=&\frac{1}{2}C_1V_B+\frac{1}{2}C_2V_R+\frac{1}{2}Li_L^2+\\&\frac{1}{2}(\alpha\varphi+\beta\varphi^3)(E_1-V_B),\end{aligned} \quad (19)$$

where the first two terms represent the electric energy of the capacitors, the third term is the magnetic energy of the inductor, and the last term describes the magnetically coupled energy of the flux-controlled memristor. Dimensionless Hamiltonians are obtained by normalizing with $C_1V_0^2$, with all dimensionless variables and parameters defined in Eq. (10):

$$\begin{cases}H_{\text{off}}=H_{C_1}+H_L+H_M=\\\qquad\dfrac{1}{2}x^2+\dfrac{\eta}{2}y^2+\left(\dfrac{1}{2}aw+\dfrac{1}{2}bw^3\right)(A-x),\\H_{\text{on}}=H_{C_1}+H_{C_2}+H_L+H_M=\\\qquad\dfrac{1}{2}x^2+\dfrac{\mu}{2}v^2+\dfrac{\eta}{2}y^2+\left(\dfrac{1}{2}aw+\dfrac{1}{2}bw^3\right)(A-x),\end{cases} \quad (20)$$

where H_{off} and H_{on} denote the total field energy of the system when the switch is open and closed, respectively. H_{C_1}, H_{C_2}, H_L, and H_M denote the energies of the capacitor C_1, capacitor C_2, inductor L, and memristor M, respectively. All dimensionless variables and parameters are defined in Section 2. The memristor is a dissipative element. Its Hamiltonian term is not physical energy but an equivalent magnetic coupling energy, serving as a mathematical metric for the system state. A nonequilibrium model is required for strict thermodynamic interpretation. To characterize the dynamical regimes and detect resonance phenomena, the time-averaged value of the Hamiltonian is introduced:

$$\langle H\rangle=\frac{1}{T}\int_0^T H(\tau)\,\mathrm{d}\tau\approx\frac{1}{N}\sum_{i=1}^{N}H_i, \quad (21)$$

where T is the total simulation time and N is the number of sampled points. The average energy $\langle H\rangle$ is calculated using Eq. (21) with total integration time $T=2000$ dimensionless units and number of sampling points $N=1\times10^5$. The first 500 time units are discarded as transient.

3 Numerical results and discussion

In the neural circuit, key physical parameters such as capacitance, resistance, inductance, and memconductance can be tuned within a finite range. Similarly, dimensionless bifurcation parameters in nonlinear dynamical models may be assigned values over a broad interval. The time series of system variables were numerically solved using a fourth-order Runge–Kutta algorithm, with a dimensionless step size of h= 0.002 and initial conditions set to (0.5, 0.2, 1.0, 0.2). For the switch-closed case, the system becomes 5D. The initial values of the five variables are set to (0.5, 0.2, 1.0, 0.1, 0.2). First, the dynamic characteristics of the basic neuron circuit were analyzed when the external control branch was disconnected, i.e., when switch S was open. In this case, the system consisted only of the four parallel branches of the main circuit, and its dynamic behavior was determined by the circuit parameters (a, b, γ, c, κ_m, κ_0, η, and A).

Fig. 2 depicts the time series evolution of the membrane potential x and its phase plane trajectories under different parameter combinations. At (a, κ_0)= (−0.06, −0.30), the system exhibited regular periodic firing, corresponding to a stable limit cycle in the phase portrait. When a was adjusted to −5.6 and κ_0 to −0.025, the firing mode transitioned to bursting, and a distinct folded structure emerged in the phase trajectory. With a further adjustment of a to −8.6, the system entered a chaotic firing state. These results confirm that, without external intervention, various neuronal firing modes, including periodic, bursting, and chaotic firing, can be generated by the designed main circuit merely by tuning its internal parameters, such as the characteristic parameter a and the bias κ_0 of the memristor. This provides a rich dynamic foundation for the subsequent introduction of external control branches.

Fig. 3 reveals the intrinsic dynamic transition mechanisms of the system through bifurcation analysis. When κ_0 was fixed at −0.025 and parameter a was

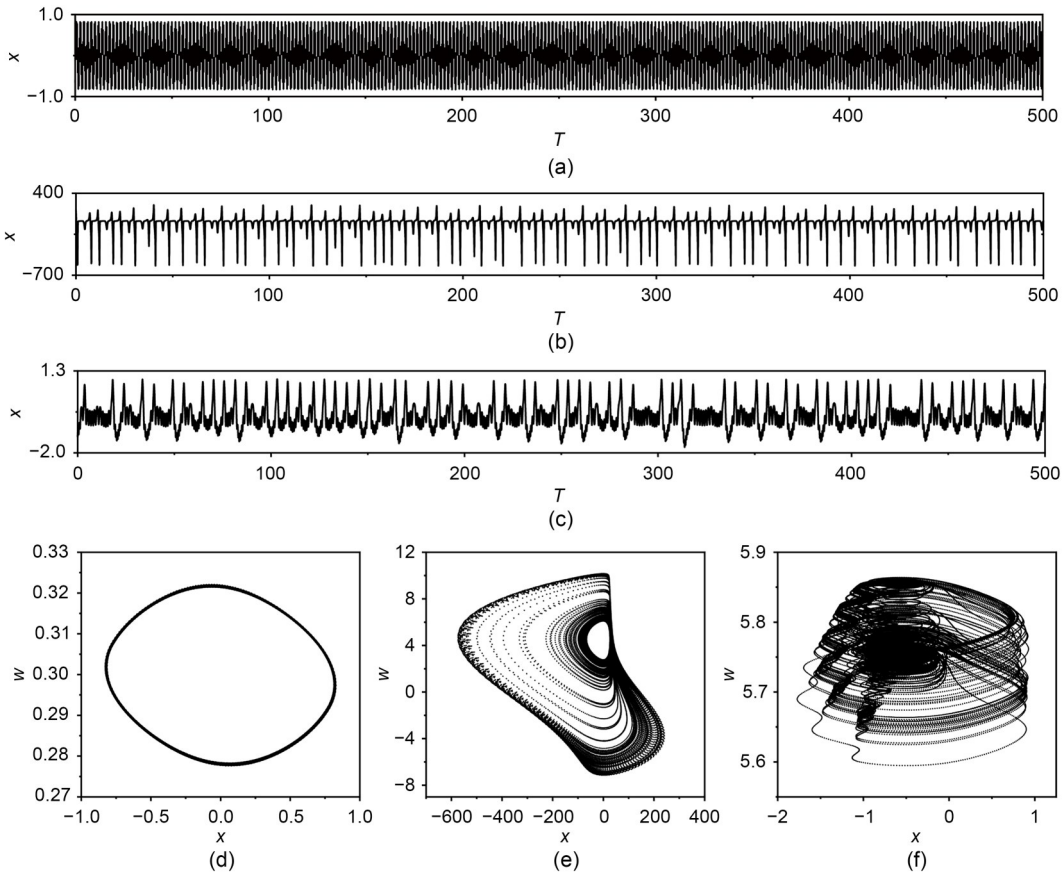


Fig. 2 With the switch open, the core neuron circuit alone can generate three distinct firing modes by tuning its internal parameters (b=0.25, γ=1.6, c=9.0, κ_m=0.1, η=0.15, and A=0.9). (a)–(c) Time series; (d)–(f) phase portraits. (a) and (d) Regular periodic firing a=−0.06, κ_0=−0.3; (b) and (e) bursting a=−5.6, κ_0=−0.025; (c) and (f) chaotic firing a=−8.6, κ_0=−0.025

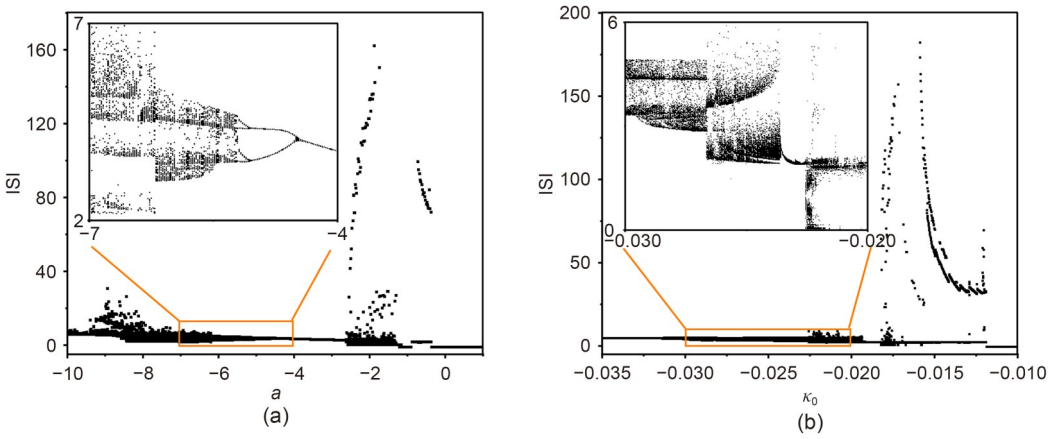


Fig. 3 Bifurcation diagrams with the switch open (b=0.25, γ=1.6, c=9.0, κ_m=0.1, η=0.15, and A=0.9). (a) κ_0=−0.025; (b) a=−5.6 (ISI: inter-spike interval)

varied, the resulting bifurcation diagram (Fig. 3a) shows that the system undergoes periodic and period-doubling bifurcations before entering chaos as a is decreased from −4 to −7. Periodic windows are observed within the chaotic region, which is consistent with the mode switching shown in Fig. 2. Similarly, with a fixed at −5.6, varying κ_0 yields a bifurcation diagram that exhibits a clear bifurcation sequence. This demonstrates the system's sensitivity to parameter variations and its rich nonlinear dynamic behavior. This thus enables the controlled switching of firing modes, which is achieved by driving the system from one attractor basin to another. The driving force is an appropriate external perturbation, such as the introduced capacitive shunting. Based on the inherent dynamic characteristics of the main circuit, the regulatory effect was further investigated after closing switch S and connecting external capacitor C_2. The external branch is directly connected in parallel with the nonlinear resistor R. Its core function is to dynamically shunt the current from Branch 4 through capacitor C_2. Inductor L in Branch 4 governs the flux decay dynamics and, together with R and C_2, determines the system's time scales and stability conditions essential for generating various firing modes, while parallel C_2 provides dynamic current shunting. The capacitance of C_2 is represented by the dimensionless parameter μ. Consequently, the circuit's equilibrium state is perturbed, and its dynamic behavior is regulated.

Fig. 4 demonstrates the immediate transition of the system's firing mode upon the switching action through time-series comparisons. Before the switch was closed at τ=500, the system remained in its initial firing state

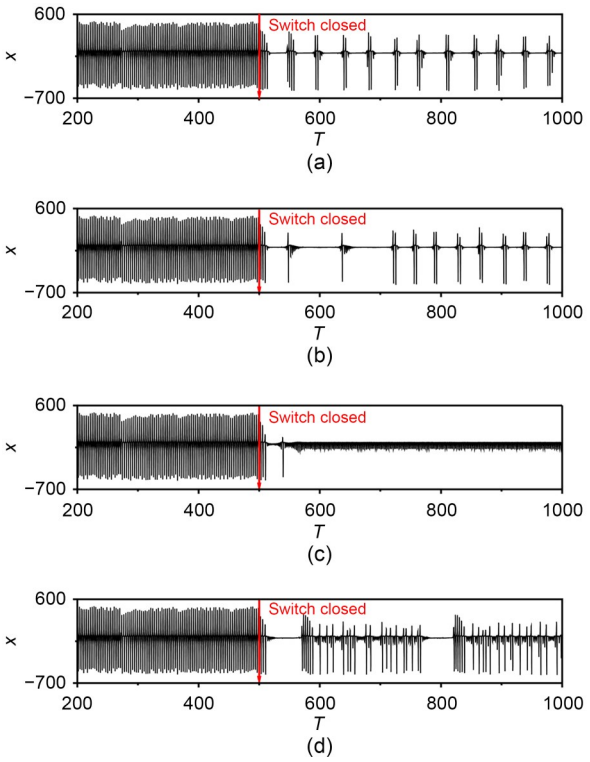


Fig. 4 Switch closes at τ=500. The final firing mode depends on the external capacitance (a=−5.6, b=0.25, γ=1.6, c=9.0, κ_m=0.1, κ_0=−0.025, η=0.15, and A=0.9). (a) μ=15.5→bursting; (b) μ=10.5→bursting (different spike count); (c) μ=5.5→regular periodic; (d) μ=0.5→chaotic

determined by the set parameters. Once the switch was closed, the circuit topology and impedance network were immediately altered by the introduction of the external branch. The system behavior then undergoes drastic evolution, with its final steady state strongly dependent on the external capacitance parameter μ.

When μ=15.5 and 10.5, the system was induced to burst, with significant modifications in oscillation amplitude, the number of spikes per burst, and interburst intervals. This indicates that fine modulation of the original dynamics can be achieved via the shunting effect of the external capacitor. When μ was reduced to 5.5, the firing pattern was completely tamed into regular periodic firing, with a drastic reduction in oscillation amplitude. Further reduction to μ=0.5 drives the system into a completely aperiodic, chaotic firing state. These results confirmed that effective and reversible switching or reshaping of neuronal firing modes can be achieved. This includes transitions from chaos to period and from period to bursting. It is accomplished solely through the continuous adjustment of a single parameter, the capacitance of the external capacitor C_2 represented by μ. This process accurately simulates the modulation of neuronal excitability in biological systems through the regulation of specific ion channel conductance, validating the precise regulatory capability of the external branch as a physical ion channel analog.

To further elucidate the continuous regulatory role of parameter μ, Fig. 5 presents an analysis with the memristor parameter a as the bifurcation parameter under different μ values. It shows that as μ decreases from 10.5 to 0.1, the route to chaos of the system changes significantly. A larger μ (Fig. 5a) allows the system to maintain periodic or quasiperiodic motion over a wider range of a. A medium μ (Fig. 5b) induces period-doubling bifurcations at an earlier stage. A smaller μ (Fig. 5c) even directly excites chaotic oscillations at small values of a. Meanwhile, the corresponding curves of the system's average energy <H> versus a are presented in Figs. 5e–5h. The energy curves are closely related to the bifurcation structure. In periodic regions, the energy changes smoothly; near bifurcation points, turning points emerge; in chaotic regions, the energy value is larger and exhibits enhanced fluctuations. This corroborates the transition of firing modes from an energy perspective and confirms that the external capacitor directly participates in the redistribution of the system's total energy through its shunting effect. The core physical mechanism of the external control branch relies on a controllable capacitive shunting path. This path forms through the parallel connection between the external branch and the nonlinear resistor R. To quantitatively reveal the influence of the shunting process, the average energies of key energy storage elements in the system are calculated. These elements include the combined capacitor C_1+C_2, the inductor L, and the memristor M. The time series and phase portraits of the system are presented in Figs. 6 and 7, along with pie charts illustrating the energy distribution among components. These results correspond to different values of μ and different stimulus amplitudes A.

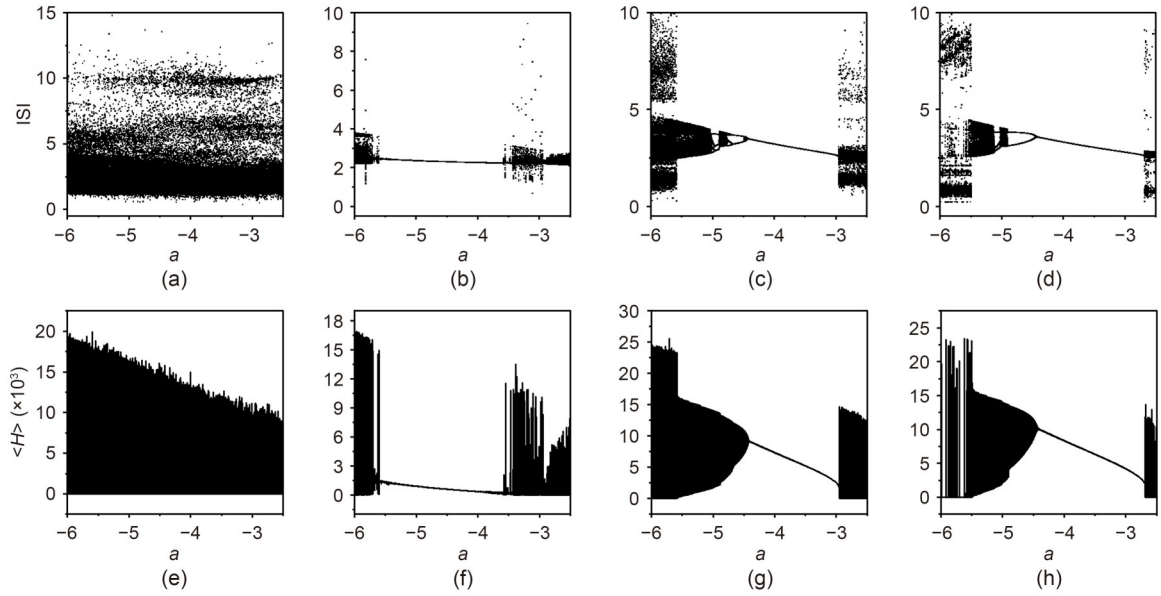


Fig. 5 Bifurcation diagrams and average energy with the memristor parameter a as the bifurcation parameter under different external capacitance parameters μ (a=−5.6, b=0.25, γ=1.6, c=9.0, κ_m=0.1, κ_0=−0.025, η=0.15, and A=0.9). (a)–(d) Bifurcation diagrams; (e)–(h) average energy <H>. (a) and (e) μ=10.5; (b) and (f) μ=5.5; (c) and (g) μ=0.5; (d) and (h) μ=0.1

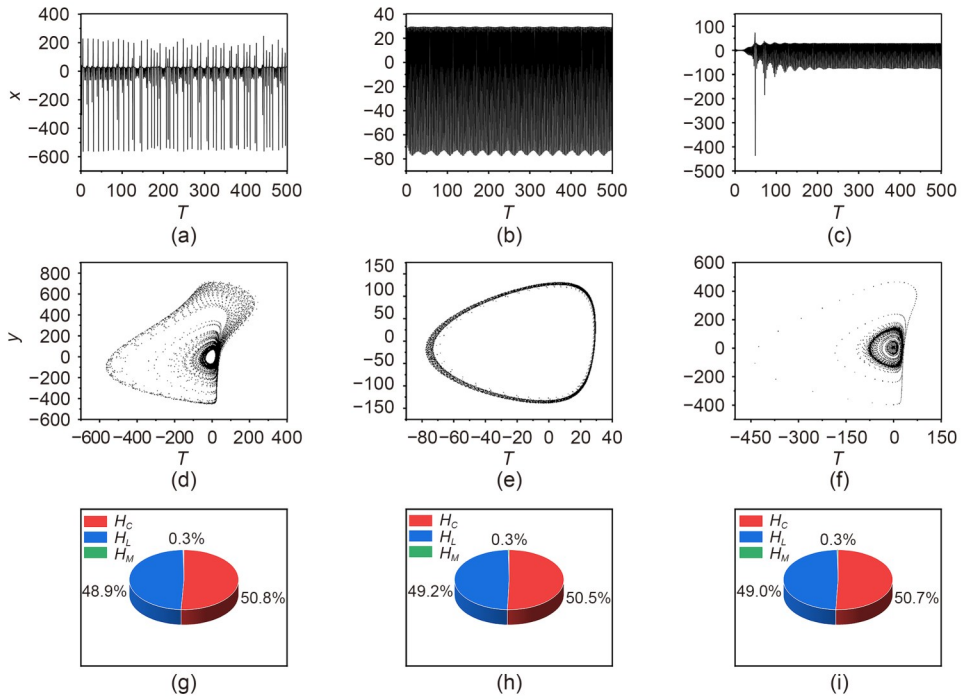


Fig. 6 Evolution of membrane potential, phase portraits, and distribution of energy proportion in a single neuron in Eq. (12) (a=−5.6, b=0.25, γ=1.6, c=9.0, κ_m=0.1, κ_0=−0.025, η=0.15, and A=0.9). (a), (d), and (g) μ=0.5; (b), (e), and (h) μ=5.0; (c), (f), and (i) μ=8.0. Each column: top—time series of membrane potential, middle—phase portrait, and bottom—energy pie chart (H_C is the energy of combined capacitor C_1+C_2). The capacitor and inductor dominate in all cases, showing that μ regulates the mode by shunting, not energy reallocation

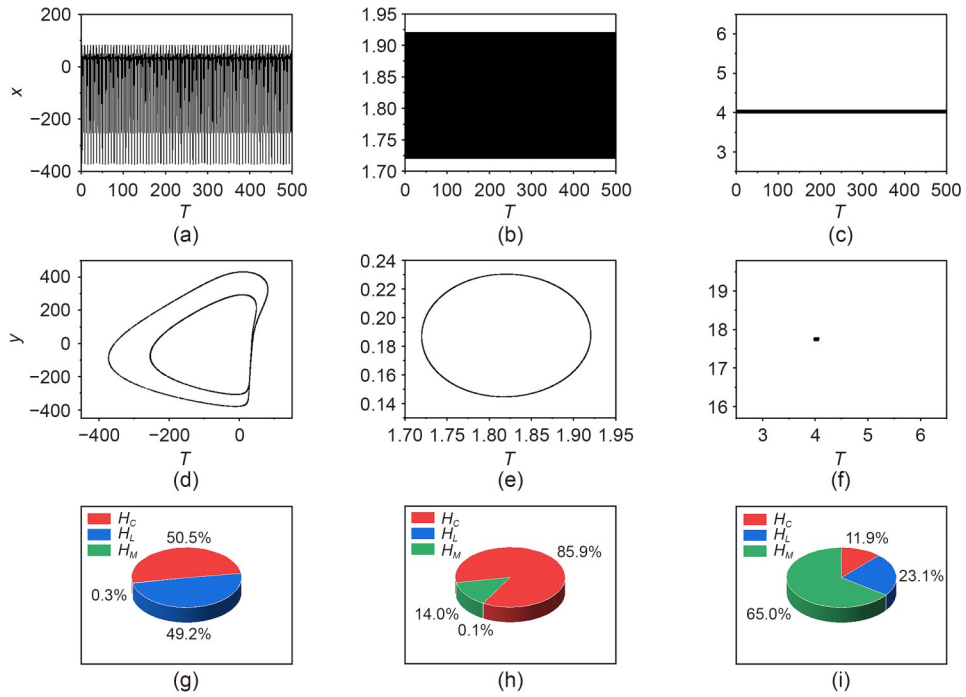


Fig. 7 Evolution of the membrane potential, phase portraits, and distribution of the energy proportion in a single neuron in Eq. (12) (a=−4.5, b=0.25, γ=1.6, c=9.0, κ_m=0.1, κ_0=−0.025, η=0.15, and μ=0.5). (a), (d), and (g) A=0.9; (b), (e), and (h) A=2.9; (c), (f), and (i) A=5.9. Each column: top—time series of membrane potential, middle—phase portrait, and bottom—energy pie chart

The results of Fig. 6 demonstrate that, across different firing states, the total system energy is predominantly allocated to the capacitor and the inductor, while the energy proportion of the memristor remains relatively small. Specifically, under the periodic firing state (μ=5), the energy stored in the capacitor is slightly lower compared to other states. When μ is set to 0.5 and 8.0, the system enters distinct firing modes, yet the overall energy distribution structure remains relatively stable with only minor adjustments. The energy proportion of the memristor exhibits almost no variation with changes in the firing state. This phenomenon reveals a core characteristic of the regulation by the external capacitance μ: the switching of firing modes in the system is primarily achieved through adjustments in oscillation amplitude and frequency, rather than through a fundamental restructuring of the energy distribution. This feature ensures that the energy framework of the system remains relatively stable during dynamical regulation within a controllable parameter range, thereby providing a physical foundation.

The results shown in Fig. 7 reveal the core regulatory role of the stimulus amplitude A on the energy distribution and oscillation characteristics of the system. When A=0.9, the system exhibits large-amplitude periodic oscillations. At this point, the total energy is almost equally distributed between the capacitor and the inductor, with the memristor accounting for a very small proportion. The system dynamics are dominated by inductor–capacitor (LC) resonance. As A is increased to 2.9, the range of periodic oscillations is significantly reduced, and a drastic transformation in the energy distribution occurs. The proportion of energy stored in the capacitor rises sharply to 85.9%, while the inductor energy is dramatically compressed to 0.1%. Meanwhile, the energy proportion of the memristor increases to 14.0%. This indicates that the system has entered a state dominated by the saturation effect of the nonlinear resistor. When A is further increased to 5.9, the range of periodic oscillations is further compressed, and a fundamental restructuring of the energy distribution is observed. The energy proportion of the memristor reaches 65.0%, making it the primary energy storage component in the system. The energy proportions of the capacitor and inductor are correspondingly greatly reduced. This series of phenomena demonstrates that the stimulus amplitude A can not only regulate the oscillation amplitude but also systematically restructure the internal energy distribution framework of the circuit. The underlying mechanism is that variations in the A value drive the system's operating point through three distinct dynamic regions: the quasilinear region dominated by LC resonance, the transition region dominated by nonlinear resistor saturation, and the strongly nonlinear region dominated by the nonlinear conductance of the memristor. This discovery forms a sharp contrast and functional complement to the regulatory mechanism of the external capacitance μ revealed in Fig. 6. The parameter μ primarily alters the oscillation modes of the circuit through capacitive shunting, including transitions between periodic, bursting, and chaotic states. In contrast, parameter A directly reshapes the dominant component of the energy distribution in the system by changing the excitation intensity. Together, they constitute a dual-dimensional mode–energy regulation system for the designed neuron circuit, providing a precisely controllable physical platform for simulating the coordinated changes in firing patterns and metabolic energy consumption of biological neurons under complex stimulation. Parameter μ adjusts the firing mode via capacitive shunting, while parameter A reshapes the energy distribution, together forming a dual-dimensional regulation that mimics biological neurons under complex stimulation and provides a flexible platform for neuromorphic circuit design.

The results in Fig. 8 reveal a key phenomenon: the average energy trends of all other energy storage components, namely, capacitor C_1, inductor L, and memristor M, are consistent with the total average system energy. In contrast, the energy evolution of capacitor C_2 exhibits a distinctly different pattern. This discrepancy can be explained by the unique physical mechanism of the external branch. The external capacitor C_2 is directly connected in parallel across the nonlinear resistor. This forms a dynamic shunting path. When the dynamical state of the system changes with the bifurcation parameter, the oscillatory characteristics of the main circuit are altered, and the current flowing through R is redistributed accordingly. The charging and discharging processes of C_2 are instantaneously coupled to the voltage across R. However, its response phase differs from that of the main LC resonant loop. This difference causes the energy accumulation rhythm of C_2 to be independent of the overall energy variation. Particularly when the system enters multiscale oscillatory states such as chaos or bursting, C_2 exhibits low

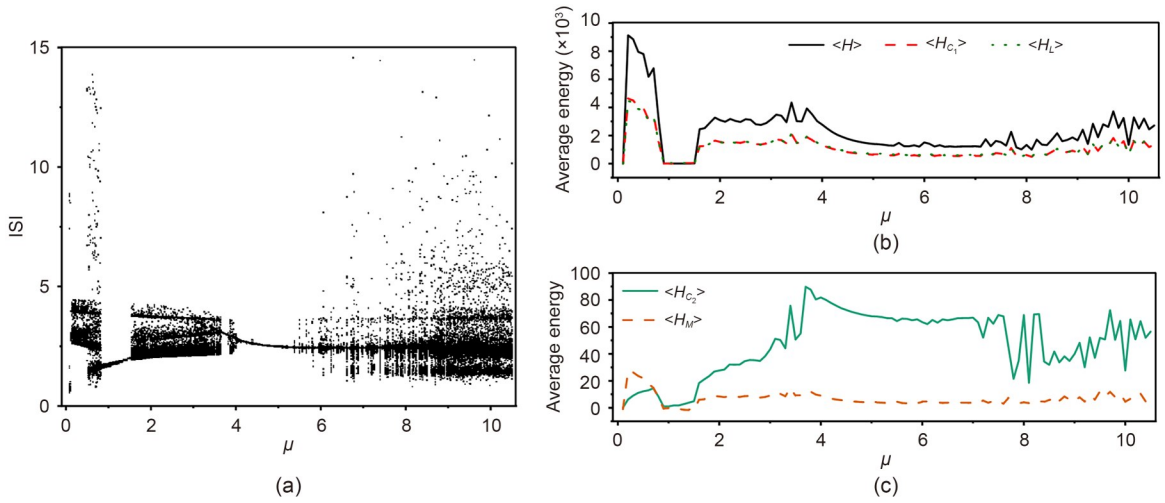


Fig. 8 (a) Bifurcation diagram with the switch closed, (b) average energies of the total system, capacitor C_1, and inductor, and (c) average energies of capacitor C_2 and memristor (a=−5.6, b=0.25, γ=1.6, c=9.0, κ_m=0.1, κ_0=−0.025, η=0.15, and A=0.9). Comparing (b) and (c), the unique behavior of C_2 indicates active perturbation of the global balance via local shunting

impedance to high-frequency components. More transient energy is absorbed by C_2. This further accentuates the uniqueness of its energy behavior. This phenomenon demonstrates that the external branch does not passively follow the oscillations of the main circuit. Instead, it acts as an active regulatory unit with an asynchronous energy response. Through specific energy exchange in the local loop, the global balance of the system is effectively perturbed. Ultimately, controllable switching of firing modes is achieved.

This study proposes a novel control method for neuronal circuits using an external capacitive shunt branch. The external capacitance parameter μ enables reversible switching among periodic, bursting, and chaotic firing modes without altering the main circuit topology. The stimulus amplitude A reshapes the internal energy distribution of the system. Together, μ and A form a dual-dimensional mode–energy regulation framework. The method reveals two physical mechanisms, namely, the local shunting effect and the asynchronous energy response. Energy analysis shows that this regulation does not disrupt the overall energy framework of the system. Compared with traditional approaches, the method offers higher precision, faster response, lower energy consumption, and easier hardware implementation. Limitations of this study include the lack of hardware validation as only numerical simulations are performed, the single-neuron scope without network synchronization, and the manual scanning of the external capacitance parameter without adaptive or closed-loop control. These limitations point to directions for future research.

4 Conclusions

This study proposes and validates a novel control method for neuronal circuits based on targeted parallel shunting using an external capacitor. The main conclusions are summarized as follows:

Effective firing pattern regulation is achieved by introducing an external capacitive branch connected in parallel with the nonlinear resistor. By continuously adjusting the external capacitance parameter μ, the system realizes controllable switching among various firing modes, including periodic firing, bursting, and chaos.

Dual-dimensional mode–energy regulation is established. While μ controls firing patterns, changes in the stimulus amplitude A reshape the internal energy distribution framework of the system, determining the dominant roles of different energy storage components. Together, these two mechanisms form a dual-dimensional regulation system for neuronal circuit dynamics.

The regulatory mechanism originates from local shunting and asynchronous energy exchange. The external capacitor C_2 exhibits dynamic characteristics distinct from those of the main system. This asynchronous energy response enables effective perturbation of the global balance of the system.

A novel physical implementation pathway is provided for constructing reconfigurable and predictable neuromorphic circuits, offering an alternative to purely software-based or complex hardware approaches.

Acknowledgments

This work is supported by the Key R&D Program of Shandong Province, China (No. 2025CXPT087) and the National Natural Science Foundation of China (No. 12402061). We sincerely appreciate the valuable comments provided by the anonymous reviewers. We are also grateful to Prof. Jun Ma from Lanzhou University of Technology, China, for his constructive suggestions.

Author contributions

Ying XU designed the research. Ying XU and Fuqiang WU processed the corresponding data. Ying XU wrote the first draft of the manuscript. Fuqiang WU helped to organize the manuscript. Ying XU revised and edited the final version.

Conflict of interest

Ying XU and Fuqiang WU declare that they have no conflict of interest.

Declaration on the use of generative AI tools

AI tools were not used when preparing the manuscript.

Data availability

The data that support the findings of this study are available from the corresponding author upon reasonable request.

References

Baumgartner C, Fuchs L, Costa A, et al., 2022. Supercurrent rectification and magnetochiral effects in symmetric Josephson junctions. *Nature Nanotechnology*, 17(1):39-44. https://doi.org/10.1038/s41565-021-01009-9

Baxevanis G, Hizanidis J, 2025. Inductively coupled Josephson junctions: a platform for rich neuromorphic dynamics. *Physical Review E*, 111(4):044214. https://doi.org/10.1103/PhysRevE.111.044214

Buzsáki G, Draguhn A, 2004. Neuronal oscillations in cortical networks. *Science*, 304(5679):1926-1929. https://doi.org/10.1126/science.1099745

Cheng S, Wang NG, Arnold DP, 2007. Modeling of magnetic vibrational energy harvesters using equivalent circuit representations. *Journal of Micromechanics and Microengineering*, 17(11):2328-2335. https://doi.org/10.1088/0960-1317/17/11/021

Chua L, 1971. Memristor-the missing circuit element. *IEEE Transactions on Circuit Theory*, 18(5):507-519. https://doi.org/10.1109/TCT.1971.1083337

Dana SK, Sengupta DC, Edoh KD, 2001. Chaotic dynamics in Josephson junction. *IEEE Transactions on Circuits and Systems I: Fundamental Theory and Applications*, 48(8):990-996. https://doi.org/10.1109/81.940189

Guo Q, Lei Z, Ren GD, et al., 2025. Memristor-coupled circuits for neurons without capacitive variable. *Chinese Journal of Physics*, 97:653-672. https://doi.org/10.1016/j.cjph.2025.06.043

Guo YT, Zhou P, Yao Z, et al., 2021. Biophysical mechanism of signal encoding in an auditory neuron. *Nonlinear Dynamics*, 105(4):3603-3614. https://doi.org/10.1007/s11071-021-06770-z

Han JP, Zhang YZ, Wang XF, et al., 2023. Ultrasound-mediated piezoelectric nanoparticle modulation of intrinsic cardiac autonomic nervous system for rate control in atrial fibrillation. *Biomaterials Science*, 11(2):655-665. https://doi.org/10.1039/d2bm01733d

Hodgkin AL, Huxley AF, 1952. A quantitative description of membrane current and its application to conduction and excitation in nerve. *Journal of Physiology*, 117(4):500-544. https://doi.org/10.1113/jphysiol.1952.sp004764

Izhikevich EM, 2006. Dynamical Systems in Neuroscience: the Geometry of Excitability and Bursting. MIT Press, Cambridge, UK. https://doi.org/10.7551/mitpress/2526.001.0001

Jia JN, Yang FF, Ma J, 2023. A bimembrane neuron for computational neuroscience. *Chaos, Solitons & Fractals*, 173:113689. https://doi.org/10.1016/j.chaos.2023.113689

Jia JN, Xie Y, Wang CN, et al., 2024. Thermosensitive double-membrane neurons and their network dynamics. *Physica Scripta*, 99(11):115030. https://doi.org/10.1088/1402-4896/ad86f6

Jia JN, Ren GD, Wang CN, 2025. Dynamics of a functional neural circuit without capacitor embedding. *Chaos*, 35(7):073127. https://doi.org/10.1063/5.0278122

Jiang CM, Liu YB, Zhang FF, et al., 2025. A novel neural circuit with a magnetic flux-controlled memristor and double capacitive membranes. *Physica Scripta*, 100(12):125212. https://doi.org/10.1088/1402-4896/ae2438

Laing CR, 2023. Chimeras on a ring of oscillator populations. *Chaos*, 33(1):013121. https://doi.org/10.1063/5.0127306

Lei Z, Ma J, 2025. Coherence resonance and energy dynamics in a memristive map neuron. *Chaos*, 35(2):023158. https://doi.org/10.1063/5.0251352

Lei Z, Guo Q, Wang CN, et al., 2025a. Continuous energy exchange between magnetic fields supporting memristive neuron firing. *Journal of Zhejiang University-SCIENCE A*, 26(8):755-770. https://doi.org/10.1631/jzus.A2500150

Lei Z, Guo YT, Ma J, et al., 2025b. Physical characteristic and dynamics in a neural circuit without using inductor and nonlinear resistor. *Chaos, Solitons & Fractals*, 199(Pt 1):116735. https://doi.org/10.1016/j.chaos.2025.116735

Lei Z, Zhang ZX, Guo Q, et al., 2026. A double-membrane neuron and circuit containing a memcapacitor. *Chaos, Solitons & Fractals*, 202(Pt 1):104688. https://doi.org/10.1016/j.chaos.2025.117436

Li CL, Yang YY, Du JR, et al., 2021. A simple chaotic circuit with magnetic flux-controlled memristor. *The European Physical Journal Special Topics*, 230(7):1723-1736. https://doi.org/10.1140/epjs/s11734-021-00181-2

Li YN, Guo Q, Wang CN, et al., 2024. A map neuron with piezoelectric membrane, energy regulation and coherence resonance. *Communications in Nonlinear Science and Numerical Simulation*, 139:108320. https://doi.org/10.1016/j.cnsns.2024.108320

Liu ZP, Zhou S, Zhu R, et al., 2025. Research on synchronization in a Josephson junction-memristor system with dual capacitive membranes. *Chaos, Solitons & Fractals*, 191: 115918. https://doi.org/10.1016/j.chaos.2024.115918

Ma J, 2026. Energy dynamics in functional neurons and neural circuits. *Journal of Lanzhou University of Technology*, 52(2): 165-172 (in Chinese).

Mishra A, Ghosh S, Dana SK, et al., 2021. Neuron-like spiking and bursting in Josephson junctions: a review. *Chaos*, 31(5):052101. https://doi.org/10.1063/5.0050526

Moon J, Leeb SB, 2016. Power electronic circuits for magnetic energy harvesters. *IEEE Transactions on Power Electronics*, 31(1):270-279. https://doi.org/10.1109/TPEL.2015.2401336

Moujahid A, d'Anjou A, Torrealdea FJ, et al., 2011. Energy and information in Hodgkin–Huxley neurons. *Physical Review E*, 83(3):031912. https://doi.org/10.1103/PhysRevE.83.031912

Nakamura Y, Pashkin YA, Tsai JS, 2001. Rabi oscillations in a Josephson-junction charge two-level system. *Physical Review Letters*, 87(24):246601. https://doi.org/10.1103/PhysRevLett.87.246601

Prezioso M, Merrikh-Bayat F, Hoskins BD, et al., 2015. Training and operation of an integrated neuromorphic network based on metal-oxide memristors. *Nature*, 521(7550):61-64. https://doi.org/10.1038/nature14441

Ranasinghe KG, Kudo K, Hinkley L, et al., 2022. Neuronal synchrony abnormalities associated with subclinical epileptiform activity in early-onset Alzheimer's disease. *Brain*, 145(2):744-753. https://doi.org/10.1093/brain/awab442

Strukov DB, Snider GS, Stewart DR, et al., 2008. The missing memristor found. *Nature*, 453(7191):80-83. https://doi.org/10.1038/nature06932

Sun GP, Yang FF, Ren GD, et al., 2023. Energy encoding in a biophysical neuron and adaptive energy balance under field coupling. *Chaos, Solitons & Fractals*, 169:113230. https://doi.org/10.1016/j.chaos.2023.113230

Uhlhaas PJ, Singer W, 2006. Neural synchrony in brain disorders: relevance for cognitive dysfunctions and pathophysiology. *Neuron*, 52(1):155-168. https://doi.org/10.1016/j.neuron.2006.09.020

Wang BC, Lv M, Zhang XF, et al., 2024. Dynamics in a light-sensitive neuron with two capacitive variables. *Physica Scripta*, 99(5):055225. https://doi.org/10.1088/1402-4896/ad37b1

Wang RB, Zhang ZK, 2007. Energy coding in biological neural networks. *Cognitive Neurodynamics*, 1(3):203-212. https://doi.org/10.1007/s11571-007-9015-z

Wu FQ, Meng H, Ma J, 2024. Reproduced neuron-like excitability and bursting synchronization of memristive Josephson junctions loaded inductor. *Neural Networks*, 169:607-621. https://doi.org/10.1016/j.neunet.2023.11.012

Xu Q, Fang YJ, Feng CT, et al., 2024. Firing activity in an N-type locally active memristor-based Hodgkin–Huxley circuit. *Nonlinear Dynamics*, 112(15):13451-13464. https://doi.org/10.1007/s11071-024-09728-z

Yan DJ, Wu FQ, Wang WS, 2026. Synchronization of neuromorphic memristive Josephson junction network and its application. *Chinese Physics B*, 35(1):010505. https://doi.org/10.1088/1674-1056/ae1456

Yang FF, Ma J, Ren GD, 2024. A Josephson junction-coupled neuron with double capacitive membranes. *Journal of Theoretical Biology*, 578:111686. https://doi.org/10.1016/j.jtbi.2023.111686

Yu F, Wang XQ, Guo RY, et al., 2025. Discrete neuron models and memristive neural network mapping: a comprehensive review. *Chinese Physics B*, 34(12):120501. https://doi.org/10.1088/1674-1056/ae0a3b

Zhang Y, Xu Y, Yao Z, et al., 2020. A feasible neuron for estimating the magnetic field effect. *Nonlinear Dynamics*, 102(3):1849-1867. https://doi.org/10.1007/s11071-020-05991-y

Zhao JY, Yu Y, Han F, et al., 2024. Dynamic modeling and closed-loop modulation for absence seizures caused by abnormal glutamate uptake from astrocytes. *Nonlinear Dynamics*, 112(5):3903-3916. https://doi.org/10.1007/s11071-023-09218-8